Since January 2020 Elsevier has created a COVID-19 resource centre with free information in English and Mandarin on the novel coronavirus COVID-19. The COVID-19 resource centre is hosted on Elsevier Connect, the company's public news and information website.

International Journal of Pharmaceutics 589 (2020) 119826

Contents lists available at ScienceDirect

International Journal of Pharmaceutics

journal homepage: www.elsevier.com/locate/ijpharm

An investigation of rhinovirus infection on cellular uptake of poly (glycerol-adipate) nanoparticles

Yasmin Abo-zeid[a,b,c,*], Gareth R. Williams[b], Lila Touabi[c], Gary R. McLean[c,d]

[a] Department of Pharmaceutics, Faculty of Pharmacy, Helwan University, Cairo, Egypt
[b] UCL School of Pharmacy, University College London, 29 – 39 Brunswick Square, London WC1N 1AX, UK
[c] Cellular and Molecular Immunology Research Centre, London Metropolitan University, 166-220 Holloway Road, London N7 8DB, UK
[d] National Heart and Lung Institute, Imperial College London, Norfolk Place, London W2 1PG, UK

ARTICLE INFO

Keywords:
Polymer nanoparticles
Poly (glycerol-adipate)
Virus infection
Nanoparticle uptake
HeLa and Beas-2B cells

ABSTRACT

Viral infections represent 44% of newly emerging infections, and as is shown by the COVID-19 outbreak constitute a major risk to human health and wellbeing. Although there are many efficient antiviral agents, they still have drawbacks such as development of virus resistance and accumulation within off-target organs. Encapsulation of antiviral agents into nanoparticles (NPs) has been shown to improve bioavailability, control release, and reduce side effects. However, there is little quantitative understanding of how the uptake of NPs into virally infected cells compares to uninfected cells. In this work, the uptake of fluorescently labeled polymer NPs was investigated in several models of rhinovirus (RV) infected cells. Different multiplicities of RV infections (MOI) and timings of NPs uptake were also investigated. In some cases, RV infection resulted in a significant increase of NPs uptake, but this was not universally noted. For HeLa cells, RV-A16 and RV-A01 infection elevated NPs uptake upon increasing the incubation time, whereas at later timepoints (6 h) a reduced uptake was noted with RV-A01 infection (owing to decreased cell viability). Beas-2B cells exhibited more complex trends: decreases in NPs uptake (*cf.* uninfected cells) were observed at short incubation times following RV-A01 and RV-A16 infection. At later incubation times (4 h), we found a marked decrease of NPs uptake for RV-A01 infected cells but an increase in uptake with RV-A16 infected cells. Where increases in NPs uptake were found, they were very modest compared to results previously reported for a hepatitis C/ Huh7.5 cell line model. An increase in RV dose (MOI) was not associated with any notable change of NPs uptake. We argue that the diverse endocytic pathways among the different cell lines, together with changes in virus nature, size, and entry mechanism are responsible for these differences. These findings suggest that NPs entry into virally infected cells is a complex process, and further work is required to unravel the different factors which govern this. Undertaking this additional research will be crucial to develop potent nanomedicines for the delivery of antiviral agents.

1. Introduction

Viral infections represent a public health problem with a major negative impact on health, socioeconomic development and are the biggest pandemic threat in the modern era (Adalja and Inglesby, 2019; Nii-Trebi, 2017). This is clearly evidenced by the 2020 COVID-19 pandemic. All the top priority emerging infectious diseases with the greatest risk of epidemic or pandemic potential are viral diseases (Nii-Trebi, 2017). There are more than 90 antiviral agents in the market (Clercq and E., 2016), but most of them are highly specific to one virus or to members of a viral family and are inactive against other viruses (Adalja and Inglesby, 2019). The high rate of virus mutation, development of antiviral resistance (Irwin et al., 2016), and preponderance of side effects with long term administration of antiviral agents (Chawla et al., 2018) are additional challenges. For example, mitochondrial toxicity recorded with nucleoside reverse transcriptase inhibitors could be lethal (Moyle, 2000). The emergence of new viruses such as SARS-CoV-2 (Pradhan et al., 2020; Zhang et al., 2020) leads to high morbidity rates (Abo-Zeid et al., 2020; Nii-Trebi, 2017; Peters and LeDuc, 1999; Pradhan et al., 2020; Shanks and Brundage, 2012; Zhang et al., 2020) since existing antivirals are often not effective. These challenges require the discovery of new approaches to control virus infections. Broad spectrum antiviral agents are one option; however, there are few of them available for clinical application, and their

* Corresponding author at: Department of Pharmaceutics, Faculty of Pharmacy, Helwan University, Cairo, Egypt.
E-mail addresses: yasmin.abozeid@pharm.helwan.edu.eg (Y. Abo-zeid), g.williams@ucl.ac.uk (G.R. Williams), lit0208@my.londonmet.ac.uk (L. Touabi), g.mclean@londonmet.ac.uk (G.R. McLean).

https://doi.org/10.1016/j.ijpharm.2020.119826
Received 6 March 2020; Received in revised form 24 July 2020; Accepted 24 August 2020
Available online 29 August 2020

administration is associated with side effects due to accumulation at off-target organs (such as that observed with ribavirin) (Franceschi et al., 2000; Soota and Maliakkal, 2014).

Nanomedicine could be considered as an alternative strategy to improve the treatment of viral infections. In the scientific literature (Lembo et al., 2018), encapsulation of antiviral agents into nanoparticles (NPs) was found to overcome several limitations of conventional antiviral agents (Szunerits et al., 2015), such as short half-lives and high frequency of drug administration (Harvie et al., 1996) and instability in vivo (Ochekpe et al., 2009). NPs can also improve the delivery of hydrophilic drug into cells (Hillaireau et al., 2006), overcome side effects (Moyle, 2000), improve bioavailability of poorly soluble antiviral agents (Gaur et al., 2014), control/sustain drug release (Lembo et al., 2013), and aid crossing the blood brain barrier (Fiandra et al., 2015); (Nowacek, 2010). However, the effect of virus infection on the uptake of NPs has not been studied in detail. To the best of our knowledge, until very recently no studies attempted to quantify NPs uptake by virus infected cells in comparison to un-infected cells. The effect of viral infection on NPs uptake is however an important consideration. NPs are mainly taken up into cells by an endocytic pathway (Foroozandeh and Aziz, 2018) and possibly a down-regulation of endocytosis because of viral infection would make NPs delivery of the appropriate antiviral agent(s) less effective.

We previously (Abo-zeid et al., 2018b) tracked the uptake of poly (glycerol-adipate) nanoparticles fluorescently labelled with rhodamine B isothiocyanate (RBITC PGA NPs) in human hepatoma cells (Huh7.5 cells) transfected with the hepatitis C virus (HCV) J6/JFH1 chimera (a recombinant HCV designed for maximum replication and virion production *in vitro*). Confocal microscopy demonstrated an enhancement of NPs uptake by infected cells in comparison to non-transfected cells, and by performing flow cytometric analyses, we found that virus transfected cells showed significantly (> 2 times) increased NPs uptake over non-transfected cells. The NPs were not decorated with any ligands to target specific receptors at the surface of Huh7.5 cells. Therefore, a change in cellular physiology due to viral infection was hypothesized to be the driving force responsible for the enhanced NPs uptake.

In this study, we have investigated if this concept could be further extended to other viruses. We tracked the uptake of RBITC PGA NPs into four models of virus infected cells: (1) HeLa cervical cancer cells infected with rhinovirus A16 (RV- A16), (2) HeLa cells infected with rhinovirus A01 (RV-A01), (3) Beas-2B bronchial epithelial cells infected with RV-A16 and (4) Beas-2B cells infected with RV-A01. Non-infected HeLa and Beas-2B cells were employed as controls. These cell lines were chosen because they have diverse biological characteristics and can be infected with RVs. HeLa is a human cervical carcinoma cell line routinely used for the propagation of RVs (Arruda et al., 1997). Beas-2B is a human bronchial epithelial cell line transformed *in vitro* to grow continuously (Reddel et al., 1988) by infection with SV40 or adenovirus-12 SV40 hybrid virus. Both HeLa and Beas-2B cell lines can be infected with RVs (Bartlett et al., 2012) as they express the major group RV receptor ICAM-1 (Greve et al., 1989) and the minor group RV entry receptor LDLR (Hofer et al., 1994).

RVs infect the airway epithelium, are considered the most frequent cause of the common cold (Mäkelä et al., 1998). They are also associated with acute exacerbations of asthma and COPD (Johnston et al., 1995; Nicholson et al., 1993; Papi et al., 2006). RVs have further been implicated in acute otitis media, sinusitis, and lower respiratory tract disease (Henquell et al., 2012; Kiang et al., 2007; Winther, 2011). In the current work, RV-A16 and RV-A01 were used as the viruses for study because they are not highly pathogenic (level II pathogens) and represent both the major and minor groups of RVs respectively, entering cells via different entry receptors and endocytic uncoating mechanisms (Schuler et al., 2014). Although both major and minor group RVs enter the endocytic pathway of cells (Fuchs and Blaas, 2009), they are thought to leave endosomes by different mechanisms (Schober et al., 1998). Thus, the use of diverse cells, viruses, entry and uncoating mechanisms should enable us to elucidate if the enhanced uptake of NPs previously reported (Abo-zeid et al., 2018b) with hepatitis C infected Huh7.5 cells is a general phenomenon applicable to all virus infected cells, or whether cell and infection type has an effect on the NPs uptake process.

2. Materials and methodology

2.1. Materials

Rhinovirus stocks, HeLa and Beas-2b cells were provided by Prof S Johnston, National Heart and Lung Institute, Imperial College London. DMEM medium, RPMI medium, fetal calf serum (FCS), non-essential amino acids (NEAA), anti-human ICAM-1-FITC, penicillin, and streptomycin were supplied by Thermo Fisher. All other materials were purchased from Sigma-Aldrich and used as supplied.

2.2. Methodology

2.2.1. Synthesis and characterization of poly(glycerol-adipate)

The polymer was synthesized following a literature protocol (Abo-zeid et al., 2018a). Briefly, poly(glycerol-adipate) (PGA) was synthesized by dissolving equal amounts (250 mmol) of glycerol and divinyl-adipate (DVA) in dry tetrahydrofuran (THF, 30 ml) in presence of a catalytic enzyme, novozyme 435 (1.25 g). The reaction mixture was stirred (overhead stirrer, 200 rpm) at constant temp (50 °C) for 24 h. This was followed by enzyme filtration and evaporation of THF to obtain a yellowish jelly-like polymer. This polymer was characterized by gel permeation chromatography (GPC) and ^{1}H NMR.

GPC were performed following our previous protocol (Abo-zeid et al., 2018a; Kallinteri et al., 2005) using a Polymer Laboratories system, employing 2 mixed bed (D) columns at 40 °C, flow rate 1 ml/min in THF, using an evaporative light scattering detector which was calibrated with 10 narrow polystyrene standards. MALDI-TOF data was collected on an Applied Biosystems QSTAR (Q-ToF) mass spectrometer for determination of polymer molecular weight and molecular weight dispersity (Đ). Briefly, polymer samples (20 mg) were dissolved in THF (2 ml) and the solutions were mixed for an hour on a roller-mixer (SRT1, Stuart) to allow the polymer to fully dissolve. This was followed by sample filtration using a syringe membrane nylon filter (0.2 μm) before the same was analyzed by size exclusion chromatography and mass spectrometer. ^{1}H NMR spectra were recorded on Bruker AVIII HD 400 MHz NMR using a BBFO + probe and are expressed in parts per million (δ) from internal tetramethylsilane. Polymer and DVA samples were dissolved in acetone-d_6 while glycerol was dissolved in DMSO-d_6 as previously reported (Abo-zeid et al., 2018a).

2.2.2. Preparation and characterization of RBITC PGA NPs

RBITC PGA NPs were prepared and fluorescent dye loading was optimized as previously reported (Abo-zeid et al., 2018b; Abo-zeid and Garnett, 2020). Briefly, RBITC (200 μl, 1 mg/ml, in methanol) was added into an aqueous phase (HEPES buffer, 10 mM, pH 7.4, 7 ml). The polymer (20 mg) was dissolved in acetone (2 ml) and then added dropwise into the aqueous phase under stirring. The sample was left to stir overnight for complete removal of the organic solvent. RBITC PGA NPs were purified by loading the sample onto a Sephacryl S-200-HR gel column (C2.5 X 40, Pharmacia, bed volume 91 ml). The column was eluted by water using an AKTA prime plus liquid chromatography system (GE Healthcare Life Sciences) at a flow rate of 1 ml/min and collected in fractions of 1.5 ml per tube. The peaks of dye labelled NPs and free dye were detected using a UV detector at 214 nm. The purified NPs dispersion was collected for particle size and zeta potential analysis. Samples were diluted in HEPES buffer (1 mM, pH 7.4) to give a count rate ranged between 50 and 300 Kcps and measurements were performed at 25 °C ± 0.1 using Malvern Zeta sizer Nano ZS (Malvern Instruments Ltd, Malvern, UK). The dye loading and encapsulation

percentages were determined by a direct method, a weighed amount of freeze dried RBITC PGA NPs was extracted in acetone: methanol (1:1 v/v). The fluorescence was measured at λ_{Ex} = 545 nm and λ_{Em} = 575 nm using a Hitachi F-4500 spectrophotofluorometer with slit widths adjusted to 5 nm. The concentration of RBITC was quantified using a predetermined calibration curve prepared in the same solvent system. Dye loading and dye encapsulation percentages were calculated using Eqs. (1) and (2) respectively.

$$\text{Dyeloading\%} = \frac{amountofdrug(mg)}{weightofnanoparticles(mg)} * 100 \quad (1)$$

$$\text{DyeEncapsulationefficacy\%} = \frac{amountofdrugentraped(mg)}{intialweightadded(mg)} * 100 \quad (2)$$

2.2.3. RVs propagation and tissue culture infectious dose 50% (TCID50) determination

HeLa cells were grown in T175 flasks in DMEM containing, FCS (10% v/v), penicillin and streptomycin solution (1% v/v). After reaching 80% confluence, cells were used to propagate the virus. The previous medium was removed, and cells were infected with RVs in the presence of DMEM and FCS (2% v/v), penicillin and streptomycin solution (1% v/v). To enhance virus attachment, the flask was gently shaken for 1 h at room temperature. Cultures were incubated for 24 h at 37 °C and 5% CO_2 where a cytopathic effect (CPE) greater than 80% was achieved. Cells were then subjected to three freeze-thawing cycles and vortexed briefly to lyse cells and release cell-associated virus. Virus was clarified by centrifugation (4000 rpm, 15 min). Supernatant containing virus was collected, aliquoted and stored at − 80°C.

RV stock solution was titred by infecting a HeLa cell monolayer (1.5×10^4 /well) in a 96 well microtiter plate using a serial diluted virus (10^{-1} to 10^{-9}) in DMEM in presence of FCS (4% v/v), penicillin and streptomycin solution (1% v/v). Plates were incubated at 37 °C and 5% CO_2 for 3 to 4 days and then wells were scored for presence or absence of CPE by microscopic examination to determine TCID50. The TCID50 refers to the final dilution of RV where there is evidence of infection of 50% of the cultured wells.

2.2.4. Cell viability after RV infection

HeLa or Beas-2B cells (4 x10^4 /well) were seeded into 24-wells plate. Culture medium [1 ml; either DMEM or RPMI with FCS (10% v/v) and penicillin and streptomycin solution (1% v/v)] was added respectively to HeLa and Beas-2B cells followed by incubation for 24 h at 37 °C and 5% CO_2. Thereafter, the culture media were removed, and cells were treated with virus solutions (1 ml) of different multiplicity of infection (MOI): 0.03, 0.3, 0.5, 0.7 and 1. The virus solution comprised RV suspended in DMEM or RPMI in presence of FCS (2% v/v), penicillin and streptomycin solution (1%, v/v). Cells were gently shaken with virus solution for 1 h at room temperature to allow attachment, followed by removal of virus solution and addition of fresh culture medium [1 ml; DMEM or RPMI with FCS (2% v/v) and penicillin/streptomycin solution (1%, v/v)] to the HeLa and Beas-2B cells respectively. Cells were incubated at 37 °C and 5% CO_2 for 24 h. This was followed by removal of culture medium from all cells and addition of Alamar Blue (AB) solution (1 ml, 36 μg/ml) into each well followed by incubation in the dark at 37 °C and 5% CO_2 for 6 h to determine the cells viability. AB solution (36 μg/ml) was prepared by dissolving AB in DMEM or RPMI containing FCS (2% v/v) and penicillin/streptomycin solution (1% v/v) for HeLa cells and Beas2B cells respectively. The fluorescence was measured at excitation and emission wavelengths of 540 and 595 nm respectively using a FLUOstar Omega multi-mode microplate reader (BMG Labtech). Negative (AB solution without cells) and positive (AB solution autoclaved for 15 min) controls were also included in the plate. Two independent experiments were performed where each sample was prepared in triplicate.

2.2.5. RV PCR to determine infection

HeLa cells infected with RV-A16 at MOI 0.5 were placed in a humidified 37 °C incubator at 5% CO_2 and were lysed with RLT buffer (Qiagen) after 2, 4, 8, 24 and 48 h of incubation. RNA was extracted from cells using the RNeasy Mini Kit (Qiagen) following the manufacturer's protocol. Purified RNA samples were reverse transcribed using a RevertAid reverse transcriptase and first strand cDNA synthesis kit (Fisher Scientific) following the manufacturer's instructions. For random hexamer primed synthesis, the reaction mix was incubated for 5 min at 25 °C followed by 60 min at 42 °C, and for Oligo (Dt)18 the synthesis reaction mix was incubated for 60 min at 42 °C.

1 μl of cDNA was added to a reaction mix of 49 μl containing PCR buffer, forward and reverse primers (RV-A16 primers were: forward: TATAAAGCTTTCCAAAGGTTGGTCGTG; reverse: TATACTCGAGCTAA GCTAACTGGTGTTC3′), deoxynucleotide triphosphates dNTPs and Taq polymerase (Fisher Scientific). After an initial denaturing step of 95 °C for 3 min, PCR was run for 40 cycles of 95 °C for 30 s, 52 °C for 30 s, 72 °C for 1 min and a final extension of 72 °C for 5 min. Similar conditions were used for amplification of the control gene glyceraldehyde-3-phossphate dehydrogenase (gapdh) using forward and reverse primers GTCTCCTCTGACTTCAA and ACCACCCTGTTGCTGTA.

2.2.6. NPs uptake by cells

HeLa or Beas-2B cells were seeded into 6-well plates (1.15×10^5/well), followed by addition of culture medium (2 ml) comprising DMEM or RPMI with FCS (10% v/v) and penicillin/streptomycin solution (1% v/v) respectively. The cells were incubated at 37 °C and 5% CO_2 for 24 h. Culture media were removed, and cells were infected with RV at MOI of 0.5 for HeLa cells and MOI of both 0.5 and 1 in the case of Beas-2B cells. Cells were gently shaken with RV for 1 h at room temperature to allow attachment, followed by removal of virus solution and addition of fresh culture medium (2 ml) containing FCS (2% v/v) before the cells were incubated at 37 °C and 5% CO_2 for 24 h. Culture medium was removed and a RBITC PGA NPs colloidal suspension (1.8 ml, 510 μg NPs) added into each well. The colloidal suspension was prepared by adding a purified NPs suspension (850 μl, 510 μg) into an equal volume of FCS, followed by incubation for 24 h. The isotonicity of the NPs suspension was adjusted with phosphate buffered saline (one tablet of PBS was dissolved in 10 ml instead of 100 ml to yield 10 times concentrated PBS solution) prior to addition to cells. Cells were incubated for different time intervals. Next, the suspension was removed, and cells were washed with PBS (2 ml, 3 washes). Cell dissociation buffer enzyme-free PBS (0.5 ml) was added to each well and the plate incubated for 10 min to detach cells. The cells were collected and centrifuged (4000 rpm, 15 min). The supernatant was removed, and cells were washed with PBS (2 ml, 3 washes). Cells were then fixed with paraformaldehyde in PBS (1 ml, 2% v/v). A set of non-infected cells were treated similarly but without addition of RV. NPs uptake was tracked using flow cytometry (Guava easyCyte 8HT, MerckMillipore). The settings of the instrument were adjusted as follows: (1) blank cells (HeLa or Beas-2B cells that were not treated with NPs or virus solution) were used to create scatter plots to observe events; (2) non-infected cells (HeLa or Beas-2B cells) previously incubated with RBITC PGA NPs for 6 h were observed by adjusting the setting of the yellow fluorescence channel. Some cells were also stained with anti-human ICAM-1-FITC by incubating on ice for 20 min with diluted antibodies followed by PBS washing and fixing with paraformaldehyde in PBS (2% v/v).

2.2.7. Statistical analysis

All statistical analysis was performed using two-way ANOVA followed by a post-hoc Tukey test. Analyses were carried out by GraphPad Prism 8.0 software at confidence level (95%, 99% and 99.9%).

3. Results

3.1. Synthesis of PGA

The successful synthesis of PGA was confirmed by ^{1}H NMR (Figure S1 and S2, Supplementary Information), with the data agreeing with the literature (Abo-zeid et al., 2018a). Size exclusion chromatography analysis gave an estimated Mn of 11.6 kDa, molecular weight dispersity Đ of 1.4, and molecular weight (Mw) of 16 kDa.

3.2. Preparation of nanoparticles:

RBITC PGA NPs were prepared by interfacial deposition and fluorescent dye loading was achieved as previously reported (Abo-zeid et al., 2018b; Abo-zeid and Garnett, 2020). The particle size was 110 ± 30 nm (diameter mean ± SD) and the polydispersity index 0.01, indicating a monodisperse sample. The zeta potential was −53.7 ± 13.3 mv indicating a stable dispersion. The encapsulation efficiency and dye loading were 54 ± 13% and 0.54 ± 0.13%, respectively. This dye loading is sufficient enough to track NPs uptake by cells using flow cytometry (Abo-zeid et al., 2018b; Abo-zeid and Garnett, 2020).

3.3. Virus infection of cells

Infection of HeLa cells is used routinely for RV propagation (Arruda et al., 1996) and infection of the human bronchial cell line Beas-2B by RV-A16 and RV-A01 has been shown previously (Bartlett et al., 2012). We made new RV preparations for these studies and demonstrated the TCID50/ml to be 2.96x10^{7} for RV-A16 and 3.9 × 10^{7} for RV-A01. To establish conditions of RV infection resulting in minimal cytotoxicity of HeLa and Beas-2B cells and allowing the investigation of NPs uptake into cells, varying multiplicity of infection (MOI) of both RV-A01 and RV-A16 was also tested. We found that an increase of MOI was associated with a decrease of cell viability in both HeLa and Beas-2B cells infected with both viruses (Table 1). The viability of HeLa cells was reduced compared to that of Beas-2B cells at higher MOI, and RV-A01 resulted in more cytotoxic effects than RV-A16 in HeLa cells. Only minor effects on the viability of Beas-2B cells were observed with both RV serotypes. For subsequent experiments with NPs, an RV MOI of 0.5 was chosen for HeLa cells and MOI of both 0.5 and 1.0 for Beas-2B cells.

To prove RV infection of cells in the absence of sustained cytopathic effects, we performed PCR to detect the RV genome. Using HeLa cells infected with RV-A16 at MOI of 0.5, RT-PCR was performed on RNA samples obtained from uninfected and RV-infected cells at several timepoints (Fig. 1). RV-A16 genome was detected in HeLa cells 24 and 48 h after initiation of infection but not at earlier timepoints. Since the same RV preparations were used to infect Beas-2B cells it was assumed that MOI of 0.5 and 1 will be sufficient to cause infection, as has been shown previously (Bartlett et al., 2012).

Table 1
Percentage viability of HeLa and Beas-2B cells after RV infection at indicated MOI. Data are shown as mean (standard deviation). Results are average of two independent experiments with three replicates in each.

MOI	HeLa cells		Beas-2B cells	
	RV-A16	**RV-A01**	**RV-A16**	**RV- A01**
0.03	99 (4)	100 (6)	106 (5)	108 (7)
0.3	99 (3)	94 (5)	106 (8)	105 (8)
0.5	94 (3)	80 (5)	101 (11)	98 (10)
0.7	90 (5)	73 (8)	101 (6)	99 (9)
1	88 (0)	66 (5)	102 (5)	97 (6)

3.4. Nanoparticle uptake by cells

Having established infection conditions that resulted in infected cells but minimal cytopathic effects, we next studied the effect of RV infection on the uptake of NPs into cells. We also investigated expression levels of the RV major group entry receptor intercellular adhesion molecule-1 (ICAM-1) on infected cells. Fig. 2A demonstrates that HeLa cells express ICAM-1, and that expression levels are not altered by RV infection. Incubation with NPs for 6 h resulted in complete uptake of NPs into HeLa cells (lower right quadrant, Fig. 2A) that were shown to be ICAM-1 positive (upper right quadrant, Fig. 2B). No significant differences in NPs uptake were observed between uninfected and RV-A16 infected cells after incubation with NPs for 6 h (Fig. 2B). However, a reduction in NPs uptake by RV-A01 infected cells was noted (Fig. 2B). This reduced uptake is most likely due to the lower viability of these infected cells as shown in Table 1.

Flow cytometry contour plots for the time course analysis of NPs uptake in the absence of ICAM-1 staining are given (Fig. 3). The lower left (LL) quadrant represents cells with a low fluorescence signal for RBITC at baseline and shifts to the lower right (LR) quadrant reflect an increase of RBITC fluorescence intensity indicative of NPs uptake. All cells, either infected or non-infected, showed a shift from the LL to LR quadrant with increased incubation times. These data are shown both as percentages of gated cells within the contour plots and as a quantitative number of cells, revealing that similar numbers of events have been analyzed within each condition (Fig. 3). The cell numbers appear slightly different because virus infection affects the cells viability, as was discussed earlier in Section 3.3.

The percentage of positive cells for both uninfected and infected cells increases with the time of incubation with RBITC PGA NPs (Fig. 4A), but there is a small reduction within infected cells. Quantitative flow cytometry analysis of NPs uptake in uninfected and infected HeLa cells is presented (Fig. 4B) as mean fluorescent intensity (MFI), from which it is apparent that uninfected cells display a comparable MFI to RV-A16 infected cells at 0, 2 and 4 h but there is a significant ($P < 0.05$) increase of MFI for RV-A16 cells at 6 h. RV-A01 infected cells demonstrated a significantly ($P < 0.01$) higher MFI than uninfected cells at all timepoints except 6 h, where the MFI was significantly ($P < 0.001$) lower. The latter is matched with the lower percentage of positive cells recorded at 6 h for RV-A01 infected cells.

Flow cytometry histograms demonstrating the uptake of NPs with time in uninfected and infected Beas-2B cells are depicted in Fig. 5A. Both uninfected and infected cells demonstrated an increase in RBITC fluorescence over control cells (cells that were not incubated with NPs, grey filled) at 1 h (red line) and 4 h (blue line) at MOI of both 0.5 and 1. Quantitative flow cytometry plots (Fig. 5B) show a similar trend of NPs uptake at MOI of 0.5 and 1. Here, uninfected cells showed a significantly ($P < 0.01$) higher uptake of NPs than infected cells after incubation for 1 h, but upon increasing the incubation time to 4 h RV-A16 infected cells showed significantly higher NPs uptake than uninfected cells ($P < 0.001$ and $P < 0.01$ at MOI of 0.5 and 1 respectively). The opposite was observed with RV-A01 infection, where NPs uptake was significantly lower than uninfected cells ($P < 0.001$ and $P < 0.01$ at MOI of 0.5 and 1).

4. Discussion

Infectious diseases include those caused by bacteria, parasites, fungi and viruses. Virus infections are considered the most challenging due to high rates of virus mutation resulting in new strains that can escape immunity and/or are resistant to antiviral agents, and adverse side effects associated with prolonged administration of antiviral agents. All of these result in reduction in the effectiveness of antiviral therapies. Encapsulation of antiviral agents into NPs has previously been reported to overcome the drawbacks of conventional therapy (Lembo et al., 2018). However, when looking at the literature we could not identify

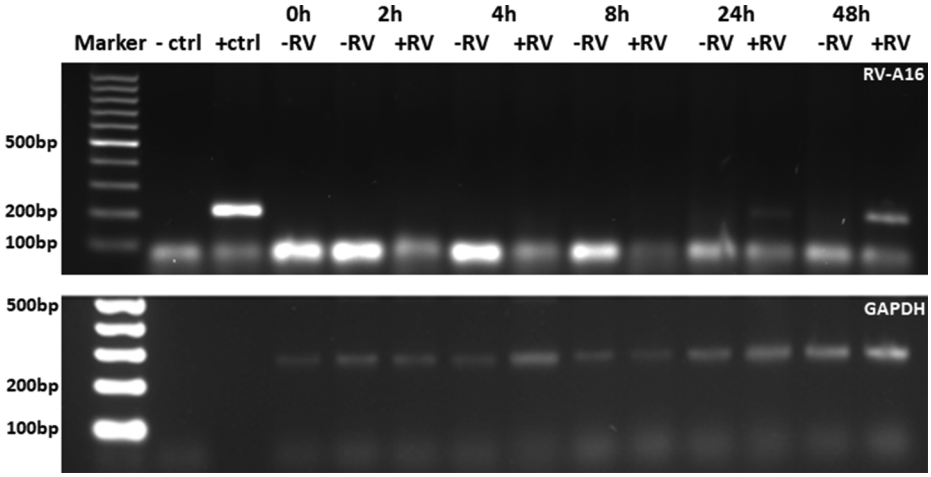

Fig. 1. RV-A16 genome is detected 24 and 48 h after infection. RT-PCR was performed on RNA obtained from HeLa cells at the indicated time-points and conditions (upper panel). –RV refers to uninfected cells and + RV to cells infected with RV-A16 at MOI 0.5. Controls used were cDNA of the RV16 genome (+ctrl) or dH2O (-ctrl). The lower panel displays the same samples where house-keeping gene GAPDH was amplified to demonstrate total RNA was present in each sample.

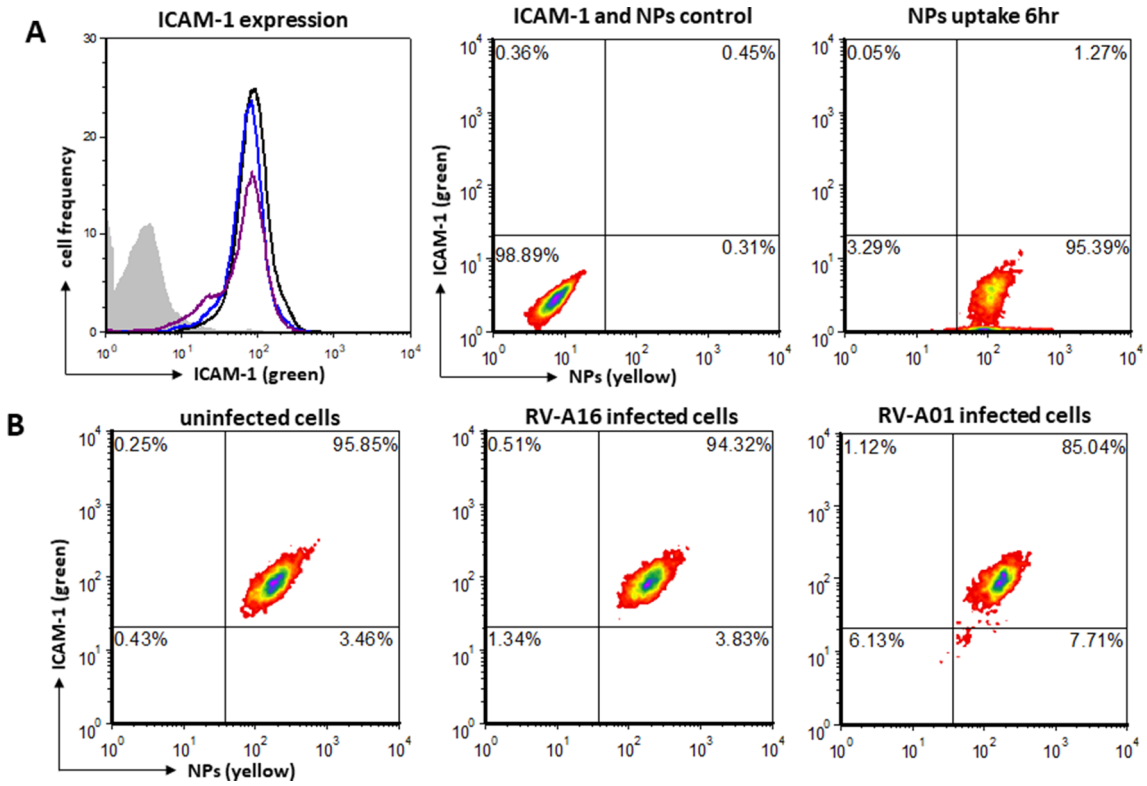

Fig. 2. Flow cytometry analysis of HeLa cells and NPs uptake. (A) ICAM-1 expression of uninfected cells (black line), RV-A16 infected (blue line) and RV-A01 infected (purple line) compared to unstained control cells (grey filled). Contour plots are shown demonstrating NPs uptake (yellow fluorescence) in the absence of ICAM-1 staining. (B) NPs uptake (yellow fluorescence) of uninfected and RV-A16 or RV-A01 infected cells co-stained with ICAM-1 (green fluorescence). Numbers represent % of gated cells within each quadrant. (For interpretation of the references to colour in this figure legend, the reader is referred to the web version of this article.)

studies investigating the effect of virus infection on the quantitative uptake of NPs. We reported in 2018 (Abo-zeid et al., 2018b) a significant two fold increase of NPs uptake in a HCV-infected liver cell line over that recorded with uninfected cells.

This study explored four different models of virally infected cells to broaden our understanding into the effect of infection on NPs uptake. We prepared fluorescently labelled RBITC PGA NPs with a dye loading that is sufficient to track the uptake of NPs by flow cytometry (Abo-zeid et al., 2018b; Abo-zeid and Garnett, 2020). These NPs were used for several reasons: they are formulated from PGA, a biodegradable and biocompatible polymer with very low cytotoxic properties (Abo-zeid and Garnett, 2020; Zhang et al., 2014; Kallinteri et al., 2005;), and RBITC is retained in the NPs for a prolonged period of time (Meng et al., 2006), allowing us to track the uptake of NPs rather than free dye (Abo-zeid et al., 2018b). RBITC dye gives a good fluorescence in the acidic pH of lysosomal compartment (Garnett and Baldwin, 1986) leading to effective detection of NPs taken up by cells using flow cytometry (Abo-zeid and Garnett, 2020; Abo-zeid et al., 2018b).

We confirmed RV infection of cells by RT-PCR and chose two levels of infection (MOI values 0.5 and 1) that resulted in infected cells but minimal cytopathic effect to allow the study of virus infection on NPs uptake. Virus infection by RV-A16 and RV-A01 either significantly ($P < 0.05$, $P < 0.01$, $P < 0.001$) increased or decreased NPs uptake compared to uninfected cells, depending on the experimental conditions. For HeLa cells, RV-A16 and RV-A01 infection elevated NPs uptake upon increasing the incubation time, but at longer timepoints (6 h) a reduced uptake was noted with RV-A01 infection. The latter was likely due to decreased cell viability.

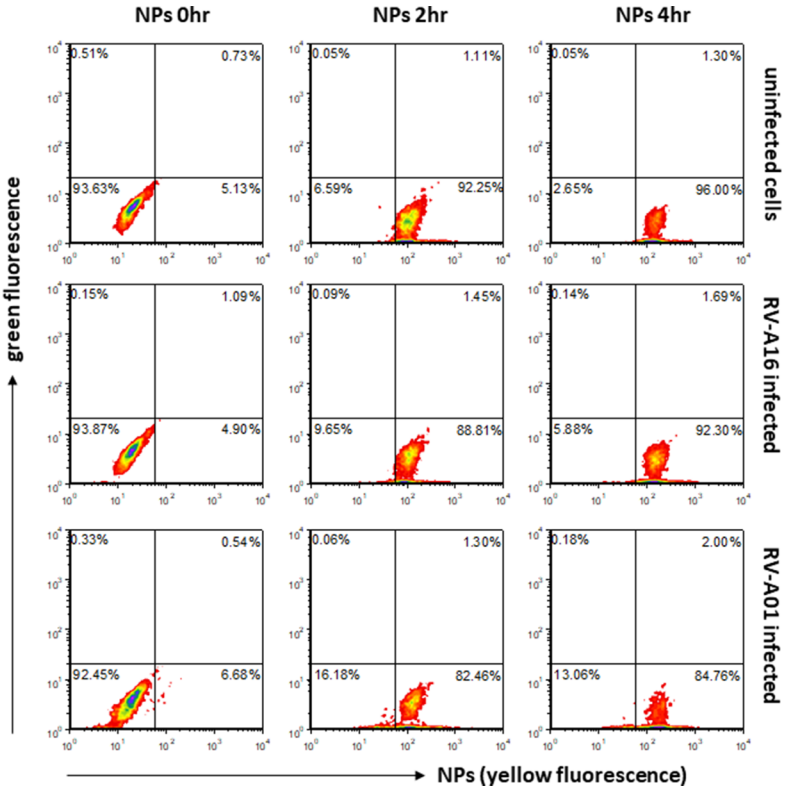

	NPs 0hr	NPs 2hr	NPs 4hr
uninfected	LL: 2189 LR: 120	LL: 131 LR: 1834	LL: 55 LR: 1993
RV-A16 infected	LL: 2586 LR: 135	LL: 207 LR: 1905	LL: 129 LR: 2025
RV-A01 infected	LL: 1702 LR: 123	LL: 274 LR: 1396	LL: 222 LR: 1441

Fig. 3. Time course analysis of NPs uptake by HeLa cells. Contour plots display NPs uptake (yellow fluorescence) of uninfected cells, RV-A16 infected cells, and RV-A01 infected cells at baseline (0hr) and for 2hr and 4hr. Numbers within contour plots represent % of gated cells within each quadrant. Numbers in the table represent quantitative cell numbers within lower left (LL) and lower right (LR) quadrants. (For interpretation of the references to colour in this figure legend, the reader is referred to the web version of this article.)

The picture with Beas-2B cells was more complex, with decreases in NP uptake observed at short incubation times following RV-A01 and RV-A16 infection. An increased incubation time (4 h) was associated with a marked decrease of NPs uptake for RV-A01 infected cells but an increase in uptake with RV-A16 infected cells. It can be argued that the reduced HeLa cell viability after infection or viral interference with the mechanism of NPs uptake due to different entry mechanisms of major (RV-A16) and minor (RV-A01) group RVs are responsible for these differences (Fuchs and Blaas, 2012). Furthermore, to observe these changes in NPs uptake, flow cytometric analyses of the MFI was required since no changes in the percentage of cells taking up NPs were seen. However, it is clear that where there is an increased uptake of NPs, this is still relatively minor when compared with our previous study (Abo-zeid et al., 2018b): when Huh7.5 cells were transfected with HCV (J6/JFH1 chimera), this resulted in a doubling of NPs uptake. J6/JFH1 is a recombinant HCV generated to maximize replication in cells *in vitro*. It was developed from one HCV variant (JFH1) providing the non-structural components and another strain (J6) providing the structural components to form the intra-genotypic HCV chimera (Lindenbach et al., 2005). It was found that J6/JFH1 chimera has both efficient RNA replication and production of virus particle that could be transfected from culture media of infected Huh7.5 cells into naive Huh7.5 cells (Lindenbach et al., 2005).

The reasons behind the difference in NPs uptake between the cell

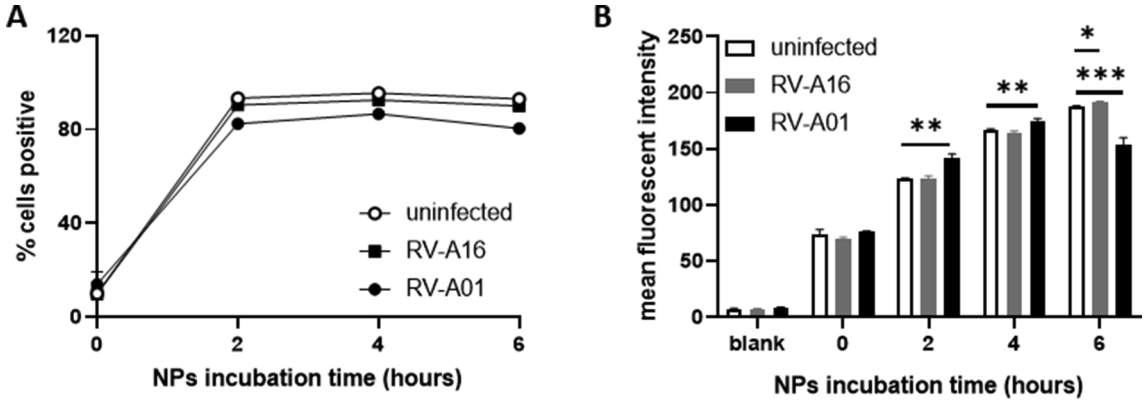

Fig. 4. Time course analysis of NPs uptake by HeLa cells. (A) Data obtained from flow cytometry contour plots display NPs uptake as the percentage of fluorescent positive cells for uninfected cells (open circle), RV-A16 infected cells (closed square), and RV-A01 infected cells (closed circle) at the indicated timepoints. (B) NPs uptake data were analysed as mean fluorescent intensity of fluorescent positive cells for uninfected cells (white), RV-A16 infected cells (grey), and RV-A01 infected cells (black) at the indicated timepoints. Data were analysed by 2-way ANOVA and significant differences are denoted with asterisks (* $p < 0.05$; ** $p < 0.01$; *** $p < 0.001$).

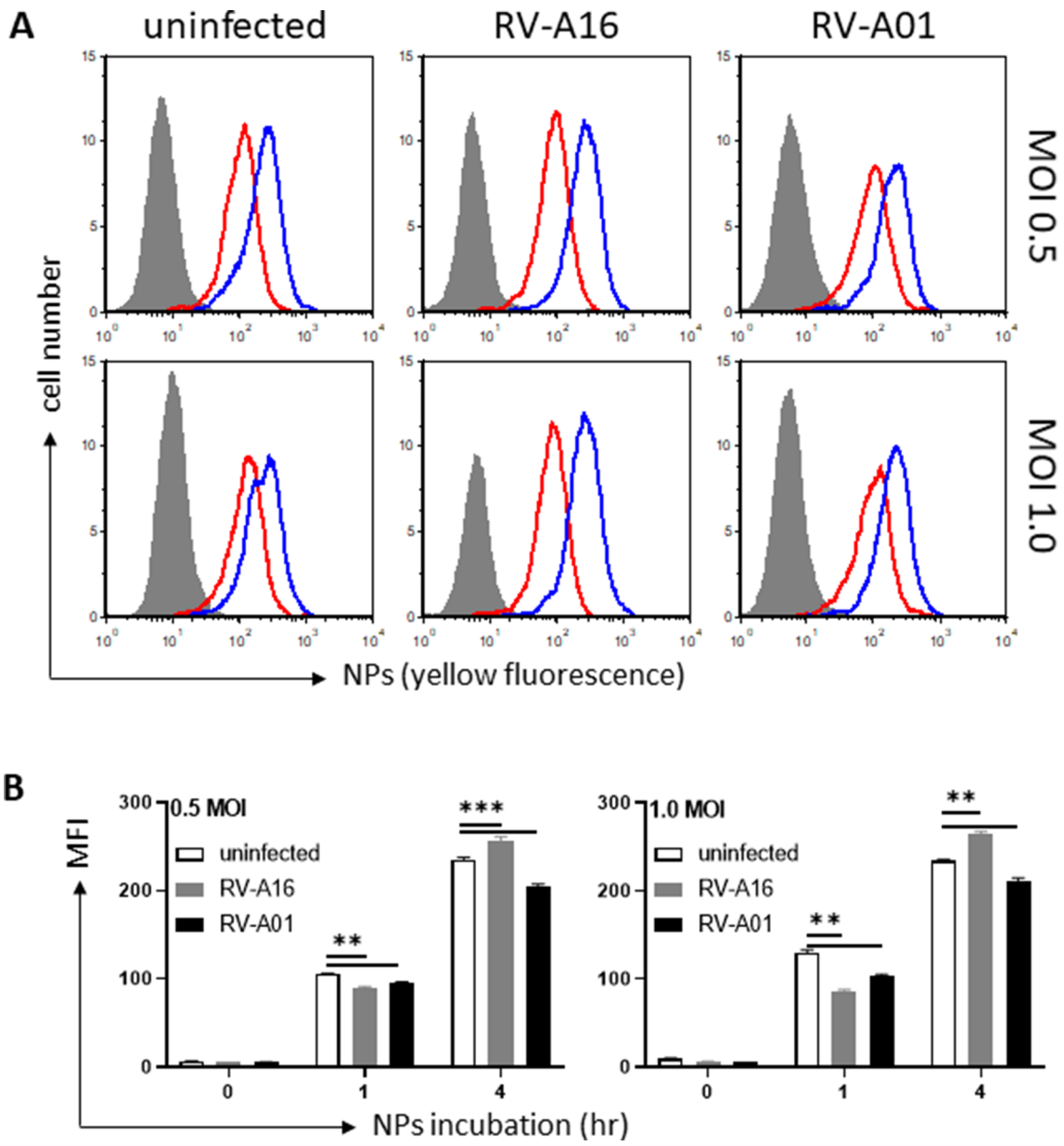

Fig. 5. Flow cytometry analysis of Beas2B cells and NPs uptake. (A) NPs uptake (yellow fluorescence) histograms of uninfected cells, RV-A16 infected and RV-A01 infected cells after 1hr (red line) and 4hr (blue line) compared to control cells without NPs (grey filled). Two different MOI were used (0.5 and 1.0). (B) NPs uptake data were analysed as mean fluorescent intensity (MFI) of fluorescence for uninfected cells (white), RV-A16 infected cells (grey), and RV-A01 infected cells (black) at the indicated timepoints and MOI. Data were analysed by 2-way ANOVA and significant differences are denoted with asterisks (** $p < 0.01$; *** $p < 0.001$). (For interpretation of the references to colour in this figure legend, the reader is referred to the web version of this article.)

lines could be both cell-related and virus-related. Firstly, considering cell-related factors, in this study we used HeLa and Beas-2B cells, selected for ease of infection *in vitro* and because they have been used extensively in previous studies. During infection in vivo, RVs infect the airway epithelium. However, primary endothelial cell cultures could not be used in this study as the cells are difficult to obtain and maintain *in vitro* for extended periods. Thus, we selected Beas-2B as a suitable alternative.

The HeLa and Beas-2B cells differ from each other and from the Huh7.5 cells used previously (Abo-zeid et al., 2018b). The main route of NPs uptake into cells is the endocytic pathway (Foroozandeh and Aziz, 2018). A previous study (Sayers et al., 2019) reported differences in the endocytic pathways between cells types, including variations in the endolysosomal morphology, localization, endocytic uptake, trafficking, recycling, endolysosomal pH, the ability of NPs to escape the endosome prior to lysosomal sequestration or exocytosis. These differences have been reported (Sayers et al., 2019) to affect the delivery of mRNA encapsulated into lipid NPs of 120 nm, and hence its expression efficiency. We expect that such differences in the endocytic pathway among HeLa, Beas-2B and Huh7.5 cells could cause variations in NPs uptake.

Virus-related factors will also be important. In our previous study (Abo-zeid et al., 2018b), Huh7.5 cells were transfected with a genetically produced chimera virus (JFH1-J6 chimera), while in the current study both HeLa cells and Beas-2B cells were infected with a whole active virus. Additionally, viral structure, size and the entry mechanism into cells could have an effect. RVs are non-enveloped viruses and have a positive-sense single stranded RNA genome that is protected by an icosahedral protein capsid built of 60 copies each of the four viral capsid proteins VP1–VP4 (Stobart et al., 2017). In contrast, Hepatitis C virus (HCV) is an enveloped (E1-E2 glycoprotein envelope) positive-

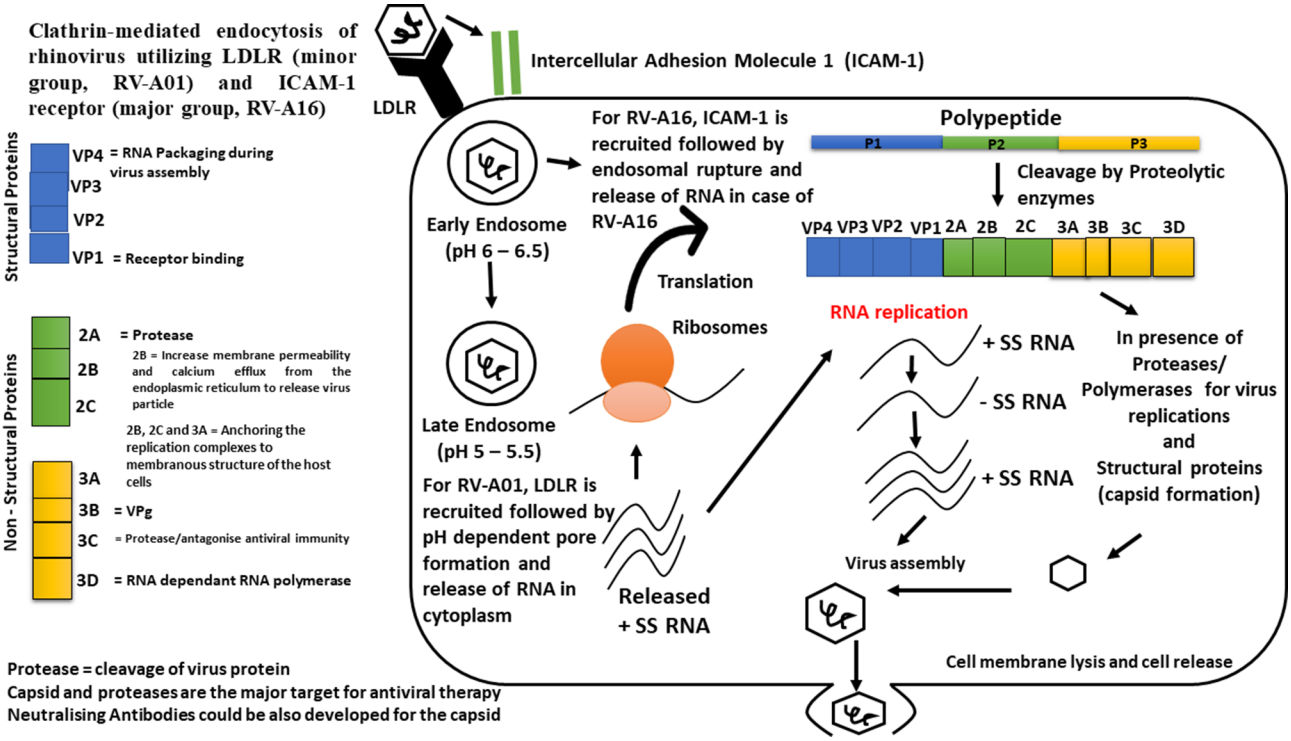

Fig. 6. Mechanism of RVs entry into cells.

sense single stranded RNA virus (Dustin et al., 2016). The particle size of RVs is around 30 nm (Fuchs and Blaas, 2012) and HCV particle size is slightly larger, ranging from 40 to 80 nm (Calattini et al., 2015; Gastaminza et al., 2010).

RVs we have used here have different mechanisms of entry into cells, as revealed in Fig. 6. RV-A16 belongs to the major group of RVs and accesses the host cell by binding to ICAM-1 receptors, while RV-A01 belongs to the minor group and binds to the low density lipoprotein receptor (LDLR) at the surface of the host cell (Fuchs and Blaas, 2012). These events are followed by clathrin mediated endocytosis, resulting in virion uncoating in the early endosome and late endosome for RV-A16 and RV- A01 respectively. This is followed by release of the RV genome into the cytosol for replication and production (Grove and Marsh, 2011). In contrast, HCV entry requires binding to four receptors: CD81, SR-B1, Claudin-1, and Occludin (Pileri et al., 1998); (Scarselli et al., 2002). Once bound to the cell, HCV is sorted by clathrin mediated endocytosis and membrane fusion in the early endosome, followed by virus uncoating and release of genetic material into the cytosol at the late endosome stage (Grove and Marsh, 2011). Virus infection might therefore affect the rate of endocytic pathway uptake of NPs, resulting in either upregulation or downregulation (or potentially have no effect). Consequently, effort should be devoted in the future to study the effect of virus infection on the endocytic pathways to understand how (or if) infection regulates the endocytic uptake of NPs.

Taken together, we hypothesis that differences in cell types, virus nature, virus size and virus entry mechanism will affect the physiology of the cell and hence have critical effects on the endocytic uptake of NPs. Therefore, future studies should be performed to elucidate the correlation between these factors and the uptake of NPs. as Additionally, research modulating the physicochemical properties of NPs (material, morphology, size, zeta potential) and surface decoration (e.g. presence of ligands for active targeting of endocytic receptors of virus infected cells) to identify the key properties controlling their uptake into virus infected cells. Finally, the specific entry receptors expressed at the surface of virus infected cells should be considered, since these could be selectively targeted to assist with the future design of NPs for selective delivery of antiviral agents.

5. Conclusions

This work involved development of four models of virus infected cells to probe the effect of virus infection on NPs uptake. It was demonstrated that virus infection in some instances caused a significant increase of NPs uptake compared to uninfected cells. For HeLa cells, RV-A16 and RV-A01 infection elevated NPs uptake upon increasing the incubation time, but at longer timepoints (6 h) a reduced uptake was noted with RV-A01 infection (owing perhaps to decreased cell viability). With Beas-2B cells more complex trends are noted, with decreases in NPs uptake (*cf.* uninfected cells) observed at short incubation times following RV-A01 and RV-A16 infection. However, an increased incubation time (4 h) was associated with a marked decrease of NPs uptake for RV-A01 infected cells while it led an increase in uptake with RV-A16 infected cells. Where increases in NPs uptake were found, they were very modest compared to results previously reported for a hepatitis C/ Huh7.5 cell line model. We argue that the diverse endocytic pathways among the different cell lines, together with changes in virus nature, size, and entry mechanism are responsible for these differences. This work raises several questions regarding the application of nanomedicine to improve antiviral therapy. To design potent medicines, it will be necessary to understand how virus entry mechanism affects the endocytic pathway of cells, and whether this can modify the uptake of NPs. Further, the subcellular signals of the endocytic pathway affected following virus infection need to be elucidated, and there is an open question as to whether virus infection affects the exocytosis of NPs. Identification of receptors specifically expressed at the surface of virus infected cells could permit the design of NPs to target infected cells, as could greater understanding of how the physicochemical properties of NPs influence uptake.

CRediT authorship contribution statement

Yasmin Abo-zeid: Conceptualization, Data curation, Formal

analysis, Investigation, Methodology, Visualization, Writing - original draft, Writing - review & editing. **Gareth R. Williams:** Conceptualization, Data curation, Formal analysis, Investigation, Methodology, Visualization, Writing - original draft, Writing - review & editing. **Lila Touabi:** Data curation, Formal analysis, Investigation, Methodology. **Gary R. McLean:** Conceptualization, Data curation, Formal analysis, Investigation, Methodology, Visualization, Writing - original draft, Writing - review & editing.

Declaration of Competing Interest

The authors declare that they have no known competing financial interests or personal relationships that could have appeared to influence the work reported in this paper.

Acknowledgment

We would like to thank the British Council and Science and Technology Development Fund in Egypt for awarding a Newton-Mosharafa Researcher Links Travel Grant to Dr. Yasmin Abo-zeid. Grant/Award Number is: Travel Grant - ID 27654.

Appendix A. Supplementary data

Supplementary data to this article can be found online at https://doi.org/10.1016/j.ijpharm.2020.119826.

References

Abo-zeid, Y., Garnett, M.C., 2020. Polymer nanoparticle as a delivery system for ribavirin: Do nanoparticle avoid uptake by Red Blood Cells? J. Drug Deliv. Sci. Technol. 56, 101552. https://doi.org/10.1016/j.jddst.2020.101552.

Abo-Zeid, Y., Ismail, N.S., McLean, G.R., Hamdy, N.M., 2020. A Molecular Docking Study Repurposes FDA Approved Iron Oxide Nanoparticles to Treat and Control COVID-19 Infection. Eur. J. Pharm. Sci. 153, 105465. https://doi.org/10.1016/j.ejps.2020.105465.

Abo-zeid, Y., Mantovani, G., Irving, W.L., Garnett, M.C., 2018a. Synthesis of nucleoside-boronic esters hydrophobic pro-drugs: A possible route to improve hydrophilic nucleoside drug loading into polymer nanoparticles. J. Drug Deliv. Sci. Technol. 46, 354–364. https://doi.org/10.1016/j.jddst.2018.05.027.

Abo-zeid, Y., Urbanowicz, R.A., Thomsonb, B.J., William L. Irvingb, A.W.T., Garnett, M. C., 2018b. Enhanced nanoparticle uptake into virus infected cells: Could nanoparticles be useful in antiviral therapy? Int. J. Pharm. 547, 572–581. https://doi.org/10.1016/j.ijpharm.2018.06.027.

Adalja, A., Inglesby, T., 2019. Broad-Spectrum Antiviral Agents: A Crucial Pandemic Tool. Expert Rev. Anti. Infect. Ther. 17, 467–470. https://doi.org/10.1080/14787210.2019.1635009.

Arruda, E., Crump, C.E., Rollins, B.S., Ohlin, A.N.N., Hayden, F.G., 1996. Comparative Susceptibilities of Human Embryonic Fibroblasts and HeLa Cells for Isolation of Human Rhinoviruses. J. Clin. Microbiol. 34, 1277–1279.

Arruda, E., Pitkäranta, A., Witek, T.J., Doyle, C.A., Hayden, F.G., 1997. Frequency and natural history of rhinovirus infections in adults during autumn. J. Clin. Microbiol. 35, 2864–2868. https://doi.org/10.1128/jcm.35.11.2864-2868.1997.

Bartlett, N.W., Slater, L., Glanville, N., Haas, J.J., Caramori, G., Casolari, P., Clarke, D.L., Message, S.D., Aniscenko, J., Kebadze, T., Zhu, J., Mallia, P., Mizgerd, J.P., Belvisi, M., Papi, A., Kotenko, S.V., Johnston, S.L., Edwards, M.R., 2012. Defining critical roles for NF- k B p65 and type I interferon in innate immunity to rhinovirus. EMBO Mol. Med. 4, 1244–1260. https://doi.org/10.1002/emmm.201201650.

Calattini, S., Fusil, F., Mancip, J., Dao Thi, V.L., Granier, C., Gadot, N., Scoazec, J.Y., Zeisel, M.B., Baumert, T.F., Lavillette, D., Dreux, M., Cosset, F.L., 2015. Functional and biochemical characterization of hepatitis C virus (HCV) particles produced in a humanized liver mouse model. J. Biol. Chem. 290, 23173–23187. https://doi.org/10.1074/jbc.M115.662999.

Chawla, A., Wang, C., Patton, C., Murray, M., Punekar, Y., Ruiter, A. de C.S., 2018. A Review of Long-Term Toxicity of Antiretroviral Treatment Regimens and Implications for an Aging Population. Infect. Dis. Ther. 7, 183–195. https://doi.org/10.1007/s40121-018-0201-6.

Clercq, E. de, E., D.C., 2016. Approved antiviral drugs over the past 50 years. Clin. Microbiol. Rev. 29, 695–747. https://doi.org/10.1128/CMR.00102-15.Address.

Dustin, L.B., Bartolini, B., Capobianchi, M.R., Pistello, M., 2016. Hepatitis C virus: life cycle in cells, infection and host response, and analysis of molecular markers influencing the outcome of infection and response to therapy. Clin. Microbiol. Infect. 22, 826–832. https://doi.org/10.1016/j.cmi.2016.08.025.

Fiandra, L., Colombo, M., Mazzucchelli, S., Truffi, M., Santini, B., Allevi, R., Nebuloni, M., Capetti, A., Rizzardini, G., Prosperi, D., Corsi, F., 2015. Nanoformulation of antiretroviral drugs enhances their penetration across the blood brain barrier in mice. Nanomedicine Nanotechnology. Biol. Med. 11, 1387–1397. https://doi.org/10.1016/j.nano.2015.03.009.

Foroozandeh, P., Aziz, A.A., 2018. Insight into Cellular Uptake and Intracellular Trafficking of Nanoparticles. Nanoscale Res. Lett. 13, 339–341.

Fuchs, R., Blaas, D., 2012. Productive entry pathways of human rhinoviruses. Adv. Virol. 2012. https://doi.org/10.1155/2012/826301.

Franceschi, L. De, Giovanna, F., Turrini, F., Ayi, K., Brugnara, C., Manzato, F., et al., 2000. Hemolytic anemia induced by ribavirin therapy in patients with chronic Hepatitis C virus infection: role of membrane oxidative damage. Hepatology 31 (4), 39–45. https://doi.org/10.1053/he.2000.5789.

Fuchs, R., Blaas, D., 2009. The enigma of yellow fever in East Africa. Rev. Med. Virol. 19, 57–64. https://doi.org/10.1002/rmv.

Garnett, M.C., Baldwin, R.W., 1986. Endocytosis of a monoclonal antibody recognising a cell surface glycoprotein antigen visualised using fluorescent conjugates. Eur. J. Cell Biol. 221, 214–221.

Gastaminza, P., Dryden, K.A., Boyd, B., Wood, M.R., Law, M., Yeager, M., Chisari, F.V., 2010. Ultrastructural and Biophysical Characterization of Hepatitis C Virus Particles Produced in Cell Culture. J. Virol. 84, 10999–11009. https://doi.org/10.1128/jvi.00526-10.

Gaur, P.K., Mishra, S., Bajpai, M., Mishra, A., 2014. Enhanced oral bioavailability of Efavirenz by solid lipid nanoparticles: In vitro drug release and pharmacokinetics studies. Biomed Res. Int. 2014. https://doi.org/10.1155/2014/363404.

Greve, J.M., Davis, G., Meyer, A.M., Forte, C.P., Yost, S.C., Marlor, C.W., Kamarck, M.E., McClelland, A., 1989. The major human rhinovirus receptor is ICAM-1. Cell 56, 839–847. https://doi.org/10.1016/0092-8674(89)90688-0.

Grove, J., Marsh, M., 2011. The cell biology of receptor-mediated virus entry. J. Cell Biol. 195, 1071–1082. https://doi.org/10.1083/jcb.201108131.

Harvie, P., Désormeaux, A., Bergeron, M.C., Tremblay, M., Beauchamp, D., Poulin, L., Bergeron, M.G., 1996. Comparative pharmacokinetics, distributions in tissue, and interactions with blood proteins of conventional and sterically stabilized liposomes containing 2′,3′-dideoxyinosine. Antimicrob. Agents Chemother. 40, 225–229. https://doi.org/10.1128/aac.40.1.225.

Henquell, C., Mirand, A., Deusebis, A.L., Regagnon, C., Archimbaud, C., Chambon, M., Bailly, J.L., Gourdon, F., Hermet, E., Dauphin, J.B., Labbé, A., Peigue-Lafeuille, H., 2012. Prospective genotyping of human rhinoviruses in children and adults during the winter of 2009–2010. J. Clin. Virol. 53, 280–284. https://doi.org/10.1016/j.jcv.2011.10.009.

Hillaireau, H., Le Doan, T., Appel, M., Couvreur, P., 2006. Hybrid polymer nanocapsules enhance in vitro delivery of azidothymidine-triphosphate to macrophages. J. Control. Release 116, 346–352. https://doi.org/10.1016/j.jconrel.2006.09.016.

Hofer, F., Gruenberger, M., Kowalski, H., Machat, H., Huettinger, M., Kuechler, E., Blaas, D., 1994. Members of the low density lipoprotein receptor family mediate cell entry of a minor-group common cold virus. Proc. Natl. Acad. Sci. U. S. A. 91, 1839–1842. https://doi.org/10.1073/pnas.91.5.1839.

Irwin, K.K., Renzette, N., Kowalik, T.F., Jensen, J.D., 2016. Antiviral drug resistance as an adaptive process. Virus Evol. 2, 1–10. https://doi.org/10.1093/ve/vew014.

Johnston, S.L., Pattemore, P.K., Sanderson, G., Smith, S., Lampe, F., Josephs, L., Symington, P., Toole, S.O., Myint, S.H., Tyrrell, D.A.J., Holgate, S.T., 1995. Community study of role of viral infections in exacerbations of asthma in 9-11 year old children. Bmj 310, 1225. https://doi.org/10.1136/bmj.310.6989.1225.

Kallinteri, P., Higgins, S., Hutcheon, G.A., St. Pourçain, C.B., Garnett, M.C., 2005. Novel functionalized biodegradable polymers for nanoparticle drug delivery systems. Biomacromolecules 6, 1885–1894. https://doi.org/10.1021/bm049200j.

Kiang, D., Yagi, S., Kantardjieff, K.A., Kim, E.J., Louie, J.K., Schnurr, D.P., 2007. Molecular characterization of a variant rhinovirus from an outbreak associated with uncommonly high mortality. J. Clin. Virol. 38, 227–237. https://doi.org/10.1016/j.jcv.2006.12.016.

Lembo, D., Donalisio, M., Civra, A., Argenziano, M., Cavalli, R., 2018. Nanomedicine formulations for the delivery of antiviral drugs: a promising solution for the treatment of viral infections. Expert Opin. Drug Deliv. 15, 93–114. https://doi.org/10.1080/17425247.2017.1360863.

Lembo, D., Swaminathan, S., Donalisio, M., Civra, A., Pastero, L., Aquilano, D., Vavia, P., Trotta, F., Cavalli, R., 2013. Encapsulation of Acyclovir in new carboxylated cyclodextrin-based nanosponges improves the agent's antiviral efficacy. Int. J. Pharm. 443, 262–272. https://doi.org/10.1016/j.ijpharm.2012.12.031.

Lindenbach, B.D.M.J.E., Syder, A.J., Wo¨lk, B., Timothy L. Tellinghuisen, Christopher C. Liu, Toshiaki Maruyama, R.O.H., Burton, D.R., McKeating, J.A., Rice, C.M., 2005. Replication of hepatitis C virus in cell culture. Science (80-.). 309, 623–626. https://doi.org/10.7124/bc.0007C9.

Mäkelä, M.J., Puhakka, T., Ruuskanen, O., Leinonen, M., Saikku, P., Kimpimäki, M., Blomqvist, S., Hyypiä, T., Arstila, P., 1998. Viruses and bacteria in the etiology of the common cold. J. Clin. Microbiol. 36, 539–542. https://doi.org/10.1128/jcm.36.2.539-542.1998.

Meng, W., Parker, T.L., Kallinteri, P., Walker, D.A., Higgins, S., Hutcheon, G.A., Garnett, M.C., 2006. Uptake and metabolism of novel biodegradable poly (glycerol-adipate) nanoparticles in DAOY monolayer. J. Control. Release 116, 314–321. https://doi.org/10.1016/j.jconrel.2006.09.014.

Moyle, G., 2000. Clinical Manifestations and Management Nucleoside Analog-Related Mitochondrial Graeme Moyle, MD, MBBS, Dip Genitourinury of Antiretroviral Toxicity Medicine. Clin. Ther. 22, 911–936.

Nicholson, K.G., Kent, J., Ireland, D.C., 1993. Respiratory viruses and exacerbations of asthma in adults. Br. Med. J. 307, 982–986. https://doi.org/10.1136/bmj.307.6910.982.

Nii-Trebi, N.I., 2017. Emerging and Neglected Infectious Diseases: Insights, Advances, and Challenges. Biomed Res. Int. 2017. https://doi.org/10.1155/2017/5245021.

Nowacek, A., 2010. NIH Public AccessNanoART, neuroAIDS and CNS drug delivery.

Nanomedicine (Lond) 4, 557–574. https://doi.org/10.2217/nnm.09.38.NanoART.
Ochekpe, N.A., Olorunfemi, P.O., Ngwuluka, N.C., 2009. Nanotechnology and drug delivery part 1: Background and applications. Trop. J. Pharm. Res. 8, 265–274. https://doi.org/10.4314/tjpr.v8i3.44546.
Papi, A., Bellettato, C.M., Braccioni, F., Romagnoli, M., Casolari, P., Caramori, G., Fabbri, L.M., Johnston, S.L., 2006. Infections and airway inflammation in chronic obstructive pulmonary disease severe exacerbations. Am. J. Respir. Crit. Care Med. 173, 1114–1121. https://doi.org/10.1164/rccm.200506-859OC.
Peters, C.J., LeDuc, J.W., 1999. An Introduction to Ebola: The Virus and the Disease. J. Infect. Dis. 179, Six-xvi. https://doi.org/10.1086/514322.
Pileri, P., Uematsu, Y., Campagnoli, S., Galli, G., Falugi, F., Petracca, R., Weiner, A.J., Houghton, M., Rosa, D., Grandi, G., Abrignani, S., 1998. Binding of hepatitis C virus to CD81. Science (80-.). 282, 938–941. https://doi.org/10.1126/science.282.5390.938.
Pradhan, P., Pandey, A.K., Mishra, A., Gupta, P., Tripathi, P.K., Menon, M.B., Gomes, J., Vivekanandan, P., Kundu, B., 2020. Uncanny similarity of unique inserts in the 2019-nCoV spike protein to HIV-1 gp120 and Gag. https://doi.org/10.1101/2020.01.30.927871.
Reddel, R.R., Ke, Y., Gerwin, B.I., McMenamin, M.G., Lechner, J.F., Su, R.T., Brash, D.E., Park, J.B., Rhim, J.S., Harris, C.C., 1988. Transformation of Human Bronchial Epithelial Cells by Infection with SV40 or Adenovirus-12 SV40 Hybrid Virus, or Transfection via Strontium Phosphate Coprecipitation with a Plasmid Containing SV40 Early Region Genes. Cancer Res. 48, 1904–1909.
Sayers, E.J., Peel, S.E., Schantz, A., England, R.M., Beano, M., Bates, S.M., Desai, A.S., Puri, S., Ashford, M.B., Jones, A.T., 2019. Endocytic Profiling of Cancer Cell Models Reveals Critical Factors Influencing LNP-Mediated mRNA Delivery and Protein Expression. Mol. Ther. 27, 1–13. https://doi.org/10.1016/j.ymthe.2019.07.018.
Scarselli, E., Ansuini, H., Cerino, R., Roccasecca, R.M., Acali, S., Filocamo, G., Traboni, C., Nicosia, A., Cortese, R., Vitelli, A., 2002. The human scavenger receptor class B type I is a novel candidate receptor for the hepatitis C virus. EMBO J. 21, 5017–5025. https://doi.org/10.1093/emboj/cdf529.
Schober, D., Kronenberger, P., Prchla, E., Blaas, D., Fuchs, R., 1998. Major and Minor Receptor Group Human Rhinoviruses Penetrate from Endosomes by Different Mechanisms. J. Virol. 72, 1354–1364. https://doi.org/10.1128/jvi.72.2.1354-1364.1998.
Schuler, B.A., Schreiber, M.T., Li, L., Mokry, M., Kingdon, M.L., Raugi, D.N., Smith, C., Hameister, C., Racaniello, V.R., Hall, D.J., 2014. Major and Minor Group Rhinoviruses Elicit Differential Signaling and Cytokine Responses as a Function of Receptor-Mediated Signal Transduction. PLoS One 9. https://doi.org/10.1371/journal.pone.0093897.
Shanks, G.D., Brundage, J.F., 2012. Pathogenic responses among young adults during the 1918 influenza pandemic. Emerg. Infect. Dis. 18, 201–207. https://doi.org/10.3201/eid1802.102042.
Soota, K., Maliakkal, B., 2014. Ribavirin induced hemolysis : A novel mechanism of action against chronic hepatitis C virus infection. World J. Gastroenterol. 20, 16184–16190. https://doi.org/10.3748/wjg.v20.i43.16184.
Stobart, C.C., Nosek, J.M., Moore, M.L., 2017. Rhinovirus biology, antigenic diversity, and advancements in the design of a human rhinovirus vaccine. Front. Microbiol. 8, 1–8. https://doi.org/10.3389/fmicb.2017.02412.
Szunerits, S., Barras, A., Khanal, M., Pagneux, Q., Boukherroub, R., 2015. Nanostructures for the inhibition of viral infections. Molecules 20, 14051–14081. https://doi.org/10.3390/molecules200814051.
Winther, B., 2011. Rhinovirus infections in the upper airway. Proc. Am. Thorac. Soc. 8, 79–89. https://doi.org/10.1513/pats.201006-039RN.
Zhang, C., Zheng, W., Huang, X., Bell, E.W., Zhou, X., Zhang, Y., 2020. Protein structure and sequence re-analysis of 2019-nCoV genome does not indicate snakes as its intermediate host or the unique similarity between its spike protein insertions and HIV-1 2.
Zhang, T., Howell, B.A., Dumitrascu, A., Martin, S.J., Smith, P.B., 2014. Synthesis and characterization of glycerol-adipic acid hyperbranched polyesters. Polymer (Guildf). 55, 5065–5072. https://doi.org/10.1016/j.polymer.2014.08.036.